

Remote Sensing Image Classification Using Deep Ensemble Learning

Niful Islam¹, Md. Rayhan Ahmed², Nur Mohammad Fahad³,
Salekul Islam⁴, A.K.M. Muzahidul Islam³,
Saddam Mukta⁵, Swakkhar Shatabda⁶

¹Department of Computer Science and Engineering, Oakland University, Michigan, USA

²Irving K. Barber Faculty of Science, University of British Columbia, Kelowna, Canada

³Department of Computer Science and Engineering, United International University, Dhaka, Bangladesh

⁴Department of Electrical and Computer Engineering, North South University, Dhaka, Bangladesh

⁵Department of Software Engineering, LUT School of Engineering Sciences, LUT University, Finland

⁶Department of Computer Science and Engineering, BRAC University, Dhaka, Bangladesh

Corresponding Author: Saddam Mukta (e-mail: saddam.mukta@lut.fi)

Abstract

Remote sensing imagery plays a crucial role in many applications and requires accurate computerized classification techniques. Reliable classification is essential for transforming raw imagery into structured and usable information. While Convolutional Neural Networks (CNNs) are mostly used for image classification, they excel at local feature extraction, but struggle to capture global contextual information. Vision Transformers (ViTs) address this limitation through self attention mechanisms that model long-range dependencies. Integrating CNNs and ViTs, therefore, leads to better performance than standalone architectures. However, the use of additional CNN and ViT components does not lead to further performance improvement and instead introduces a bottleneck caused by redundant feature representations. In this research, we propose a fusion model that combines the strengths of CNNs and ViTs for remote sensing image classification. To overcome the performance bottleneck, the proposed approach trains four independent fusion models that integrate CNN and ViT backbones and combine their outputs at the final prediction stage through ensembling. The proposed method achieves accuracy rates of 98.10 percent, 94.46 percent, and 95.45 percent on the UC Merced, RSSCN7, and MSRSI

datasets, respectively. These results outperform competing architectures and highlight the effectiveness of the proposed solution, particularly due to its efficient use of computational resources during training.

Keywords: Classification, Ensemble, Fusion Model, Remote Sensing Image

1 Introduction

Remote sensing (RS) refers to the technique of accumulating information about an entity from a certain distance, commonly using satellite, unmanned aerial vehicle (UAV), or other platforms [1]. Remote sensing imagery provides a unique opportunity for retrieving information through the process of image interpretation and classification since it covers a large geographic area with high temporal frequency. The increasing volume of RS data has opened new studies and research opportunities in the fields of natural resource exploration, environment management, earthquake prediction, urban planning, and many more [2]. All these sources of RS images generate a need for an automatic process for knowledge mining. Using image classification techniques, this vast amount of images can be organized according to their context [3].

Among popular image classification techniques, deep learning is the most popular one. Convolutional Neural Networks (CNNs) are the most common deep learning architectures for image recognition tasks. These deep learning models are specifically designed to process and extract features from image data, making them immensely effective in tasks such as object detection, image classification, and facial recognition [4]. CNNs are composed of layers that learn and represent visual patterns collectively. These layers include fully connected, pooling, and convolutional ones. One of the most difficult challenges in training CNNs is the need for large labeled datasets [5]. Transfer Learning, however, has become a potent method to get around this restriction and boost the effectiveness of training CNNs. Transfer learning entails using pre-trained models that have been optimized on smaller, task-specific datasets after being trained on massive datasets like ImageNet. Transfer learning enables CNNs to take advantage of the pre-trained model's representations and generalized patterns, which are shared by many different types of images [6]. This knowledge transfer enables the CNN to learn more effectively on the target dataset, even when the labeled data is limited. Transfer learning also aids in combating overfitting because the trained model has already acquired useful representations from a large body of data [7]. The initial layers of the pre-trained CNN's weights are frozen during the transfer learning process, and only the top layers are retrained using the target dataset. By using this method, the model is able to retain the low-level features it has already learned while adjusting to the specific features found in the new dataset.

One of the biggest limitations of CNNs is that its limited ability to capture global context [8]. Vision transformers (ViT) came as a solution to this problem [9]. The ViT introduces a new paradigm for image understanding, inspired by the success of transformers in natural language processing [10]. This architecture gets around CNN limitations by capturing the distant dependencies and taking into account an image’s overall context. ViT works by dividing an image into smaller patches, which are then linearly projected by multiplying with a learnable weight matrix. These tokens are then fed into a typical transformer architecture made up of feed-forward neural networks and self-attention layers. The model gains the ability to focus on pertinent patches and draw out valuable representations from the image during training. The learned representations can then be used for a variety of downstream tasks such as image classification, object detection, and segmentation. The ViT has displayed astounding performance on a variety of benchmarks, competing with or even outperforming CNNs in some tasks. On massive datasets like ImageNet, it has produced state-of-the-art results in image classification, demonstrating its potential as a potent substitute for conventional CNN architectures. Following the outstanding performance of ViT, many vision transformer bases architectures have also emerged, such as data efficient image transformer (DeiT) [11], swin transformers [12], and others.

Since the feature extraction mechanisms of CNNs and Vision Transformers are fundamentally different, their integration allows a model to exploit the complementary strengths of both architectures and achieve strong image recognition performance [13]. Although hybrid models that combine multiple feature extractors often outperform standalone architectures, our study reveals a performance bottleneck in this approach. Experimental analysis shows that adding more CNN and ViT components results in insignificant performance improvements while increasing the computational cost, mainly due to overlapping feature representations that limit the contribution of additional extractors. To overcome this limitation, we propose an ensemble strategy based on a soft voting mechanism. In this work, we present a fusion architecture that integrates CNN and ViT models for remote sensing image classification, where four distinct fusion models composed of CNN and ViT backbones are trained independently and later ensembled through soft voting to produce the final prediction. The proposed method has been evaluated on the UC Merced, RSSCN7, and MSRSI datasets, and the results demonstrate outstanding classification performance across all datasets. In addition, we compare the proposed approach with several existing architectures and provide a detailed discussion that explains the reasons for its superior classification performance. In conclusion, the main contributions of this work are summarized as follows.

- We have presented a novel architecture for classifying remote sensing images that is comprised of vision transformers and convolutional neural networks (CNNs). The architecture addresses the performance bottleneck issue by integrating a soft voting

mechanism.

- The proposed model is tested on three benchmark datasets of remote sensing images, and the model performs significantly well in classifying different types of images.
- We have presented a comparison with different models and made a conclusive discussion about their performance.

The rest of the article is organized as follows. The summary of the related works in the field of remote sensing images is presented in Section 2. Section 3 contains the detailed description of the proposed method, followed by the results in Section 4. The article terminates in Section 5.

2 Related Work

Aerial classification from the remote sensing data has gained a lot of attention due to the comprehensive exploration of the locations and environmental monitoring. The advancement of AI can provide accurate classification of scenarios from remote sensing images, analyze the features of those scenarios, and improve the effectiveness and scalability of remote sensing applications.

In recent studies, a combination of DL and ML models has been widely used for segmentation, localization, or classification purposes. Shen et al. [14] developed a dual-model deep features fusion technique for classifying the remote sensing images from 4 different datasets. They utilized two CNNs for feature extraction. The features were then passed through a cascade global–local network (ACGLNet) that filtered out repeated background information. The proposed method obtained a satisfactory accuracy of 98.14% in UCM, 94.44% in AID, 99.50% in PatternNet, and 96.02% in the OPTIMAL-31 dataset, respectively. Hilal et al. [15] proposed a new deep transfer learning-based fusion model named DTLF-ERSIC. It extracted features from Discrete Local Binary Pattern (DLBP), ResNet, and EfficientNet which were merged later. This strategy was found to provide better performance compared to the base classifiers. Huang et al. [16] combined supervised (SA) and unsupervised alignment (UA) techniques to propose a new bidirectional sample alignment technique for remote sensing scene classification. The supervised approach completes the feature alignment between source and target samples using the label of the samples, whereas the unsupervised approach aims to align the global features without demanding class information. They conducted these experiments on several datasets and obtained satisfactory performance. Ghadi et al. [17] performed object categorization and scene classification on remote sensing data using feature fusion techniques. They implemented a hybrid model employing fuzzy c-means, CNN, and FCN in order to segment and classify the images. The evaluation of the proposed techniques reports a mean

accuracy of 97.73% on the AID dataset, 98.75% on the UCM, and 96.57% on the RESIEC dataset, respectively. Alem and Kumar [18] developed a land cover and land use classification system using the deep learning approaches over the remote sensing images. They utilized CNN to interpret the images as well as extract the features, and developed a fine-tuned transfer learning model for classification. This model is evaluated on the UCM dataset and obtains an accuracy of 88.10%. Al-Jabbar et al. [19] developed a modified Darknet-53 architecture using ebola optimization for scene classification and enhancing the security of smart cities. The Darknet-53 architecture was utilized to extract the feature from the remote sensing images of RSSCN7 dataset. Ebola optimization was used to optimize the hyperparameter and finally, graph convolution was used to perform the classification task. The proposed method attains a sublime accuracy of 99.52%. Thirumaladevi et al. [20] experimented with transfer learning with two state-of-the-art CNN models (AlexNet and VGG). The model extracted features with pretrained CNN feature extractor which are then passed to the SVM for final classification. Out of the two CNN models compared, VGG16 was found to produce better results. Vinaykumar et al. [21] introduced a new method named optimal guidance-whale optimization algorithm (OG-WOA) for selecting relevant features in order to reduce the overfilling problem. They extracted features from AlexNet and ResNet which are then passed through OG-WOA where irrelevant features are deleted. Finally, the refined features make the classification through a shallow BiLSTM network. The proposed framework produced an excellent classification performance in classifying remote sensing images. Wang et al. [22] proposed a custom model made of residual dense attention block (RDAB) and coordinate attention (CA) module. RDAB module integrates dense connections as well as skip connections, leveraging the advantages of DenseNets and ResNets. Wang et al. [23] presented a novel two-stage based CNN architecture that consists of MS-Res block and Split Attention block. MS-Res block is made up by modifying the inception block with a hierarchical residual connection. The Split Attention module is integrated for cross-channel feature mapping. These two blocks are combined parallelly to construct the final model. Wang et al. [24] introduced a model named Large kernel Sparse ConvNet weighted by Multi-frequency Attention (LSCNet) for classifying remote sensing images. LSCNet effectively addresses the need for larger receptive fields by utilizing two parallel convolutional layers. These layers extract features simultaneously and then combine them, eliminating the need for a large convolutional layer which reduces resource consumption. Additionally, the integration of an adaptive sparse optimization strategy and multi-frequency attention module enhanced performance and optimized the network. Although the proposed model is relatively small at 10.69 MB, it required 500 epochs to train due to the absence of transfer learning. Wang et al. [25] developed a three-stream architecture named Multi-stage Self-Guided Separation Network (MGSNet). This network consists of three branches: the background branch, the main branch, and the target branch. The authors extracted the

target and the background representations with adaptive threshold segmentation which are passed to the background and target branches, respectively. The main branch, on the other hand, received the original image. The three streams extracted features simultaneously which are fused before classification. Since each stream consists of only three convolution blocks, the model is extremely lightweight. Zhang et al. [26] proposed a newly developed architecture named spatial-logical aggregation network (SLA-NET) for classifying hyperspectral images. This network consists of two key modules (i.e., the feature extractor and the adaptive feature fusion). The feature extractor consists of the spatial extractor stream and the morphological extractor stream. The two streams extract features simultaneously, which are fused with the adaptive feature fusion mechanism.

Recently, computer vision transformers have emerged as a powerful tool that outperforms the classical CNNs in the majority of the image classification datasets [9]. Therefore, it is being extensively applied for recognizing remote sensing images. Chaib et al. [27] extracted features from four ViT models and merged the feature vectors to obtain a raw dataset. Since employing multiple models can result in redundant features, they applied feature selection technique for data scrubbing. Finally, the classification was done through support vector machine (SVM). Swin Transformer is another recent addition in the computer vision transformer family that incorporates a shifted window and hierarchical feature fusion for image recognition [12]. Hao et al. [28] presented a two-stream Swin Transformer network for RS image classification. In the first stream (original stream), the image is directly passed through the Swin Transformer, and the second stream (edge stream) passes the image through an edge detector made of sobel operator before passing it to the Swin Transformer. The seams are fused afterward to construct a robust classifier. Xu et al. [29] proposed a knowledge distillation based architecture named ET-GSNet. In this model, the vision transformer works as the teacher model and ResNet18 as the student model. They evaluated ET-GSNet on AID, NWPU-RESISC45, UCM, and OPTIMAL-31 datasets.

While both CNNs and vision transformers have their own limitations, researchers explored combining both methods for effective classification. Roy et al. [30] fused hyperspectral and LiDAR data for remote sensing classification. They extracted CNN features, tokenized them into patch tokens, and fused these with a LiDAR-derived CLS token using a multihead cross-patch attention mechanism within a transformer encoder. Xu et al. [31] merged CNN and transformer and designed a dual-branch network where a Dynamic-CNN branch captures local multiscale features and a Gaussian Transformer branch captures global dependencies, which are interactively fused via a cross-attention module. Similarly, Wang et al. [32] combined transformer and gist CNN techniques to design a fusion network for multimodal remote sensing data. Their architecture began with a feature reconstruction module that decomposed hyperspectral and SAR (Synthetic Aperture Radar) inputs to reduce redundancy. Then, a transformer-based spectral

module extracted global channel dependencies, while a gist CNN-based spatial module captured fine-grained spatial details. Finally, these distinct features were fused through a cross-attention fusion mechanism. Since the fusion models benefit from both CNNs and transformers, they produce better accuracy than single-stream architectures.

Fu et al. [33] utilized a graph convolutional network for semi-supervised remote sensing image classification. They introduced example-feature graph techniques for preserving the local geometrical distribution of the data. This experiment was evaluated on four public datasets and demonstrated a satisfactory performance. Yu et al. [34] developed an attention-based mechanism to perform the aerial scene classification. They introduced the attention GAN to address the scarcity of training data. After augmentation, a context-aggregation-based feature fusion architecture is applied to obtain the contextual features from the images of four publicly available datasets. Finally, the loss is calculated to yield the model's performance. Yang et al. [35] designed a new method to evaluate the quality of remote sensing images using the node entropy calculation. The node module selection selects the images node from the labeled data, calculates the node entropy between the node images and unlabeled images, and locates the same distance node images in the same boundary. This study utilized this technique on AID and RSSCN7 datasets and obtained the accuracy of 92.48% and 90.37%, respectively. An efficient way to evaluate the proposed ViTs and CNNs combination is by comparing it with the existing ensemble methods that use mixed backbones. For example, several researchers have shown that ensemble methods that integrate CNNs with better ViT models are beneficial for various applications [36–39]. A study achieved remarkable results in biodiversity image classification by using ensembles of Data-Efficient Image Transformers (DeiT), in which a CNN was utilized as a teacher model for a ViT student [36]. To diagnose bronchial asthma, a hybrid ensemble model that combines CNNs and ViTs was also created. It uses a hierarchical framework that captures features throughout receptive fields [37]. Additionally, a fusion model that integrated CNNs and ViTs was presented in a recent work for the multi-label chest X-ray image classification [38]. Another study reports increased accuracy and decreased error rates by employing a CvT model, obtaining reliable accuracy [39]. Our proposed ensemble approach is aligned with this research trend and highlights the advantages of combining model fusion with a global context, capturing an effective approach to improve the efficacy and robustness of image classification tasks.

Table 1: Comparison with existing works.

Paper	Dataset	Model	Drawbacks	Our Solution
Yu et al. [34]	UCM, AID, RSSCN7	Attention GAN	No comparison with other transfer learning models, lower classification accuracy.	An ablation study comparing other approaches is present. Has higher classification accuracy.
Shen et al. [14]	UCM, AID, PatternNet, OPTIMAL-31	ResNet50, DenseNet121, Attention Cascade Net	No transfer learning employed. Therefore, has a large number of trainable parameters.	We integrated pretrained models. Therefore, total trainable parameters are slightly above 8 million.
Ghadi et al. [17]	AID, UCM, ResisC45	fuzzy c-means, CNN, Feature fusion.	Incorporates machine learning algorithms that cannot be sped up by GPU. Therefore, very inefficient to train	The model can be sped up by GPU.
Alem and Kumar [18]	UCM	Custom CNN model	Has low classification accuracy.	Achieves higher classification accuracy.
Wang et al. [22]	UCM, AID	Multiple-Instance Learning with a Residual Dense Attention CNN	Too much complexity and requires more computational cost.	Less computational cost with 8.13M trainable parameters and 80 epochs of training.
Yang et al. [35]	AID, RSSCN7	Node Entropy	No proper prediction task using deep learning approach.	Experimented with numerous DL architectures and configured the optimal model.

Paper	Dataset	Model	Drawbacks	Our Solution
Thirumaladevi et al. [20]	UCM, SIRI-WHU	VGG, Support Vector Machine (SVM)	Low classification performance and consumed a very high number of iterations for training.	Has higher performance. Moreover, consumes only 80 epochs of training in total.
Vinaykumar et al. [21]	AID, NWPU, UCM	AlexNet, ResNet, BiLSTM, Whale Optimization	No investigate alternative feature selection methods to confirm that the proposed method is the most effective.	Comparison with prior literature validates the effectiveness of our feature fusion method.
Huang et al. [16]	NWPU-RESISC45, AID, RSSCN7, WHU-RS19	Supervised alignment, Unsupervised alignment	Incorrect pseudo-labeled target samples due to performance bottleneck.	Solved performance bottleneck with soft voting.
Jabbar et al. [19]	RSSCN7	DarkNet-53, Ebola optimization	The paper lacks in-depth analysis and clarity regarding GCN implementation.	Provide a transparent and in-depth analysis of the methodology.
Wang et al. [24]	UCM, AID, NWPU-RESISC45	LSCNet	Does not integrate transfer learning. Hence, requires 500 epochs to train.	We employ transfer learning, which reduces the training epoch to 80.

An analysis of the research papers along with the limitations that our approach addresses is presented in Table 1. The thorough analysis carried out in this study has exposed several significant shortcomings in the majority of the research works that have been done in the field. These research works specifically suffer from three major flaws, including a bottleneck caused by the integration of traditional feature extraction modules that are resistant to GPU acceleration, decreased accuracy, and excessive resource consumption during the training phase. While some research explored combining CNNs with vision transformers, they consume high resources to train due to the number of parameters of the architectures. Therefore, we developed a solution that alleviates the bottleneck and mitigates the high training costs of previous approaches. Our solution adopts a delicately designed architectural design that eliminates the bottleneck issue to

alleviate these problems. Our approach involves deploying four different models, each of which can be trained in parallel, and which together have a modest 8.1 million trainable parameters. The training regimen consists of 80 epochs, with each model receiving 20 epochs. Remarkably, this method leads to state-of-the-art performance, representing a significant advancement in the field.

3 Proposed Method

This section discusses the data preprocessing and augmentation steps as well as the proposed model architecture in detail. Figure 1 presents an overview of the process.

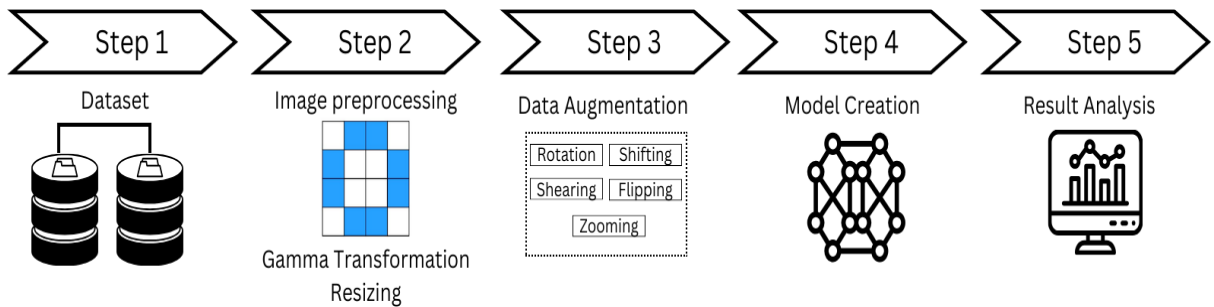


Figure 1: Flow diagram of the proposed method.

3.1 Data Preprocessing

Image preprocessing is one of the crucial steps for enhancing image classification performance. As remote sensing images are captured from a distance, they often suffer from limited visibility, especially for small and dark objects. One of the common methods used to address this is gamma transformation [40]. In gamma transformation, as shown in Eq 1, a non-linear function maps the input image r to an output image s by raising each pixel value to a power of γ and multiplying it with a constant c . Since the images of both datasets are captured from the satellite, some images lack visibility. Therefore, when γ is greater than 1, it intensifies the brightness of the images, leading to improved visualization of small, dark objects. Nevertheless, a higher γ degrades the image quality by inflating the high-intensity pixels. Hence, after a meticulous experiment, the gamma transformation was performed with a γ value of 1.1 and c set to 1.

$$s = c \times r^\gamma \tag{1}$$

We have employed transfer learning to enhance the resource efficiency of the feature extraction process. These state-of-the-art models, trained on ImageNet, typically require images to be resized to 224×224 for architectural compatibility [41]. This standardized

input size is used throughout our experiments. In addition, ViT adaptive patch embedding can tackle input sizes, whereas CNN models modify their adaptive pooling layers to ensure compatibility in the input dimension. However, since the original resolution of the images in both datasets is higher, downscaling to this size could lead to performance degradation due to the loss of fine details. To address this, we resized the images to 448×448 using nearest-neighbor interpolation. This careful resizing ensured compatibility with the pretrained feature extractor by maintaining a consistent scale factor of two and preserving crucial details in the remote sensing images. Next, the pixel values were normalized by dividing each pixel by 255. Image normalization ensures faster convergence. Additionally, some real-time data augmentation was implemented to augment the training images. The augmentation methods include:

- **Random Rotation:** Images were randomly rotated by 40 degrees clockwise or anticlockwise.
- **Random Horizontal and Vertical Shifts:** Images are arbitrarily shifted horizontally and vertically by a maximum of 20%.
- **Random Shearing:** Shear transformation applied to the input images with a maximum shear angle of 0.2.
- **Random Zooming:** Images were randomly zoomed in and out in a range of 20%.
- **Horizontal Flipping:** Some randomly selected images were flipped horizontally.

3.2 Model Architecture

As shown in Figure 2, the proposed model ensembles four fusion models through a soft voting mechanism. Each fusion model consists of two streams. The first stream is the transformer stream, and the second stream is the CNN stream. The subsequent sections describe the architecture of the streams along with the fusion process.

3.2.1 Transformer Stream

The transformer stream incorporated a pretrained ViT-Base model trained on the ImageNet1K dataset. ViT-Base is the smallest ViT architecture proposed by Dosovitskiy et al. [9]. The pretrained transformer feature extractor then followed a batch normalization (BN) to effectively reduce the training process. The BN layer has a momentum of 0.99 and an epsilon of 0.001 to enhance the training stability and generalization capability. Right after the BN, a Multi-Layer Perceptron (MLP) was added that consisted of three fully connected (FC) layers of 512, 256, and 121 neurons respectively with ReLU activation function. The first FC layer applied L2 kernel regularization with a coefficient of

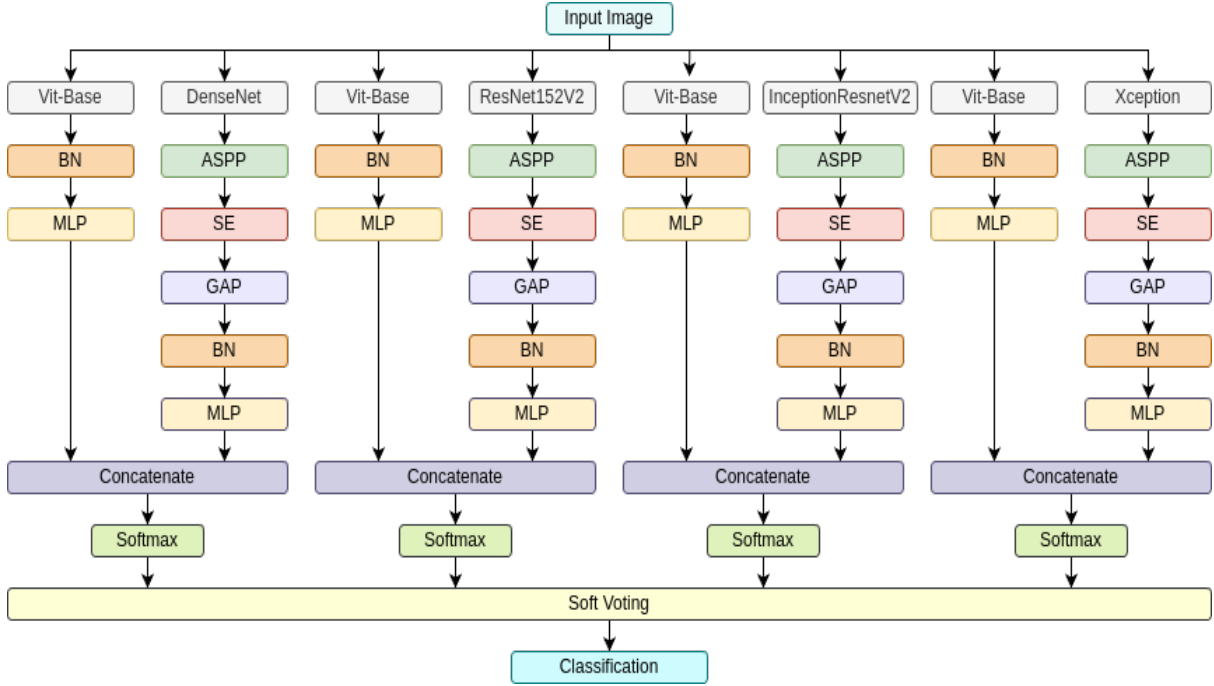


Figure 2: Proposed model architecture.

0.016, L2 activity regularization with a coefficient of 0.006, and L1 bias regularization with a coefficient of 0.006. The gradual reduction in the number of neurons across the MLP layers was designed to progressively distill and refine the learned features.

3.2.2 CNN Stream

Each fusion model-specific CNN stream included a pretrained CNN feature extractor for extracting distinguishing features from the input images. After the CNN feature extractor, an Atrous Spatial Pyramid Pooling (ASPP) module was integrated for extracting multi-scale features. ASPP captures multi-scale contextual information by applying atrous (dilated) convolutions with different dilation rates. The change in the dilation rates expands the receptive field without increasing the kernel size, which ensures resource efficiency. Since remote sensing images have both fine and large features that contribute to the classification process, ASPP is essential for accurately detecting and analyzing these features. As presented in Figure 3, the ASPP module included several parallel dilated convolutions ranging in dilation rates (2, 3, 5, and 7) on a 3×3 kernel. According to the experiment, the ASPP module dramatically increased the classification performance. Additionally, since the feature extractor was trained on ImageNet, which contains imagery dissimilar to the remote sensing data, some feature maps do not contribute equally to the classification process. Therefore a squeeze-and-excitation (SE) block was incorporated after the ASPP module to emphasize the important feature maps and reduce the influence of those with lesser contribution. SE block is an attention mechanism that imposes channel attention on the feature maps [42].

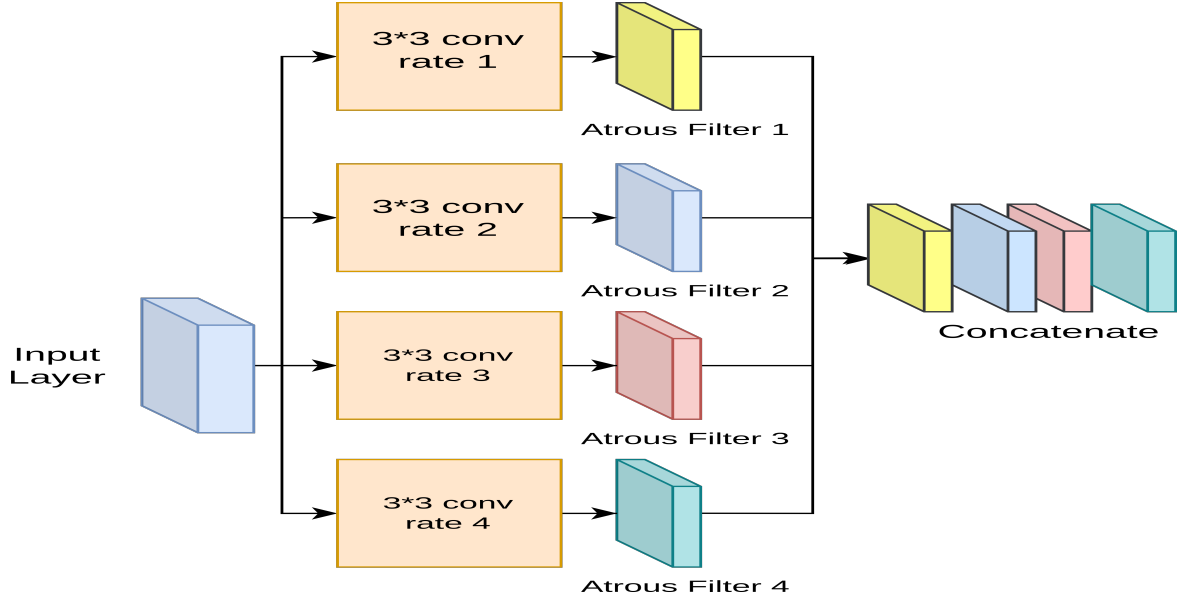


Figure 3: The ASPP module used in the model.

The attention block operates through three major steps: compression, excitation, and recalibration. During the compression step, depicted in Eq 2, the spatial dimensions of a feature map are reduced using global average pooling. Let F_c represent a feature map with height H and width W . The channel summary, denoted by scalar c_c , is computed by averaging the values of the channel F_c .

$$c_c = \frac{1}{H \times W} \sum_{i=1}^H \sum_{j=1}^W F_c(i, j) \quad (2)$$

In the excitation step, shown in Eq 3, the scalar c_c is processed through two fully connected layers. Let W_1 and W_2 denote the weights of the first and second layers, respectively. The first layer uses ReLU activation, while the second layer uses a sigmoid activation function. The excitation phase produces the channel weight e_c , which is then used to scale the feature map, resulting in the recalibrated feature map R_i . The recalibration process is defined in Eq. 4.

$$e_c = \sigma(W_2 \times ReLU(W_1 \times c_c)) \quad (3)$$

$$R_i = e_c \times F_c \quad (4)$$

For converting 2D feature maps into 1D feature vectors, global average pooling (GAP) was employed. GAP returns a single value by taking the average of the feature map. As per the experiment, GAP layer increases the classification accuracy compared to the flattening layer by remarkably reducing the number of parameters. The feature vectors are then passed through a BN layer and an MLP block. The configuration of the BN and

MLP is the same as that in the transformer stream.

3.2.3 Fusion Process

This fusion process blends the complementary strengths of both streams, taking advantage of the spatial information captured by the CNN stream and the global context modeling provided by the transformer stream. In this process, the outputs from the transformer stream and the CNN stream were concatenated and passed through softmax layers for classification. Therefore, each fusion model had the classification ability. The four fusion models vary in only the CNN feature extractor module. Four pretrained CNN models were integrated in fusion models namely DenseNet121 [43], ResNet152V2 [44], InceptionResnetV2 [45] and Xception [46].

3.2.4 Soft Voting and Classification

Soft voting is an ensemble technique used to combine predictions from various models [47]. Instead of making discrete predictions, each model in soft voting provides class probabilities. To obtain a final prediction, these probabilities are then averaged, which typically produces more reliable and accurate classification decisions. The proposed model performed soft voting on the four fusion models that were constructed previously. Since in our scenario, summing up the class probabilities and calculating the average probability makes no difference in the overall classification performance, we take the summation of the four predictions and the class label with the highest probability is declared as a prediction.

3.2.5 Hyperparameters

Each fusion model was compiled on Adam optimizer and the categorical cross-entropy loss function. The training process of all the models lasted for 20 epochs. In total, the four models consumed 80 epochs of training. The learning rate for each model was set to 0.001. The batch size for all the models was 64. The weights and biases of the feature extractor of the fusion models were initialized with ImageNet pre-trained weights and set to non-trainable.

4 Results and Discussion

This section discusses the results obtained from the proposed model. In addition to that, it also presents an ablation study.

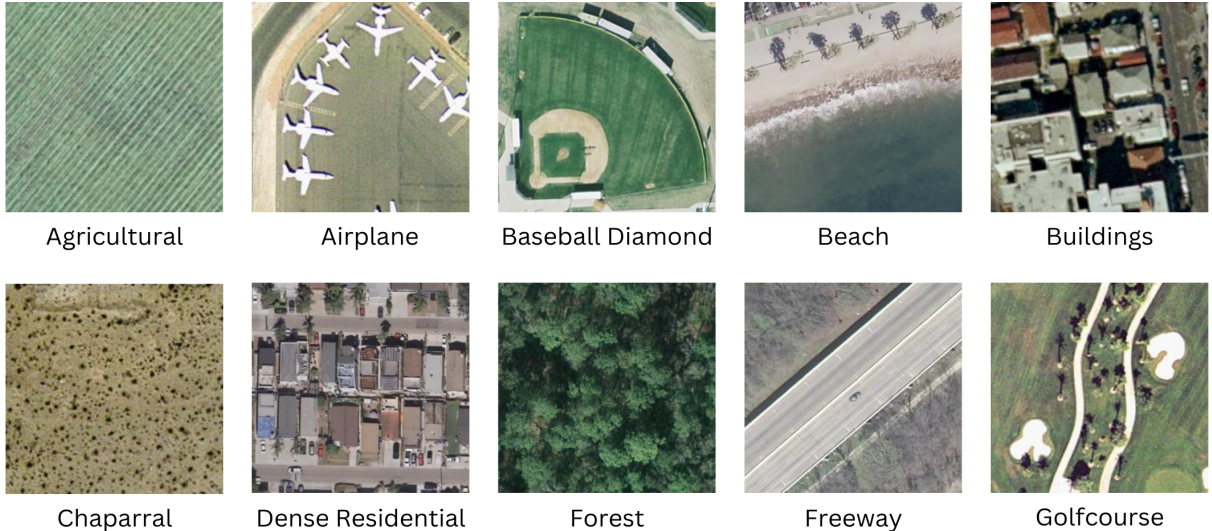


Figure 4: Samples from the UCM dataset.

4.1 Dataset Description

For evaluating the model’s performance, three benchmark datasets are selected. The first dataset is the UC Merced Land Use (UCM) Dataset, one of the most popular datasets in the field of remote sensing, consisting of 21 classes of various land cover types formed by the US Geological Survey [48]. With a total of 2100 images of with 100 images from each class, this fully balanced dataset contains high-resolution aerial images captured from a satellite of size 256×256 pixels. RSSCN7 dataset, on the other hand, is comprised of 2800 images of 7 classes acquired from Google Earth throughout multiple years time span [49]. The images of this dataset are of size 400×400 . Lastly, the MSRSI dataset consists of five types of remote sensing images, including VHR, MSI, SAR, MAP, and PAN, collected from sources like Google Maps [50]. For this experiment, we considered only the VHR type of images to match the other datasets. The dataset contains 30,000 VHR images with 15 class labels, evenly distributed across each class. A sample of the UCM, RSSCN7, and MSRSI datasets is presented in Figure 4, 5, and 6, respectively.

4.2 Result Analysis

Before the final soft voting, each fusion model was trained and evaluated on the same datasets. The accuracy of the models paired with different transformers is presented in Table 2. Each model was trained using the same hyperparameters. The results show that the CNNs paired with ViT (ViT Base) outperformed the Swin Transformer (SwinT) [12] and the Data-efficient Image Transformer (DeiT) [11]. Additionally, the fusion model constructed with ViT Base and DenseNet121 performed the best on the UCM dataset, while pairing ResNet152V2 with ViT achieved the highest accuracy on the RSSCN7 and MSRSI datasets. However, combining Xception with transformers resulted in lower



Figure 5: Samples from the RSSCN7 dataset.

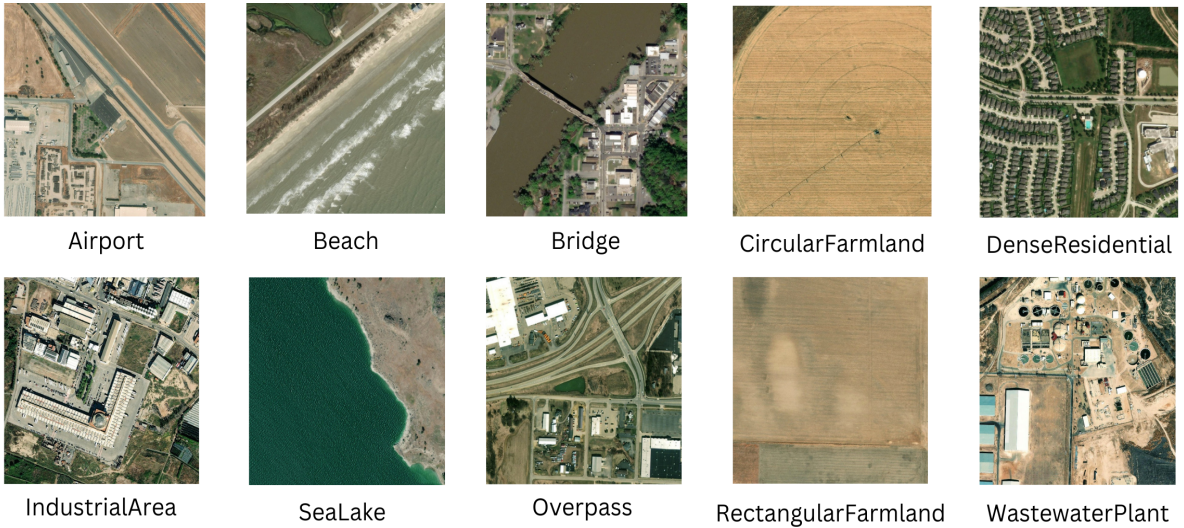


Figure 6: Samples from the MSRSI dataset.

mean and median accuracy compared to DenseNet121 and ResNet152V2. This difference in performance could be attributed to the fact that both DenseNet121 and ResNet152V2 propagate previously extracted features through multiple layers to retain minute details important for classification. Xception, while propagating features, also includes a point-wise convolution block to shrink the size of feature maps and reduce computational cost. This process may inadvertently discard fine features essential for the decision-making process in remote sensing images.

Various evaluation metrics were considered when evaluating the final model. The confusion matrix presents a detailed overview of the model’s performance at a granular level. The confusion matrices for the three datasets on the proposed model are presented in Figure 8, 9 and 10. The metrics illustrate that the model can classify the majority of the images correctly. On the UCM dataset, two mobile home parks were misclassified

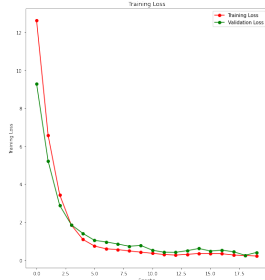
Table 2: Performance of each fusion model before soft voting with different transformer models. RSS refers to the RSSCN7 dataset and MSR refers to the MSRSI dataset.

Model	ViT			SwinT			DeiT			Trainable Parameters	Epoch
	UCM	RSS	MSR	UCM	RSS	MSR	UCM	RSS	MSR		
DenseNet-121	95.47	91.07	91.03	95.00	90.54	82.17	94.05	89.82	77.92	1.5M	20
ResNet-152V2	92.38	91.25	91.95	91.42	91.61	84.77	93.33	92.50	85.50	1.9M	20
Inception ResNetV2	92.86	89.46	92.25	91.66	80.00	83.58	90.71	87.86	84.17	2.3M	20
Xception	91.90	87.32	89.75	88.81	89.29	87.15	89.82	91.19	82.03	2.3M	20

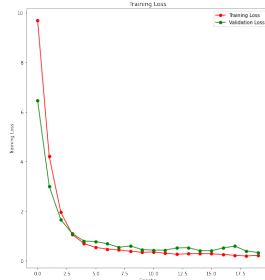
as dense residential areas, and two others were misclassified as medium residential parks. This misclassification is primarily attributed to high inter-class similarity. Additionally, no other classes in the UCM dataset experienced more than one misclassification. On the RSSCN7 dataset, however, seven grass images were misclassified as fields. This result indicates that global features negatively impacted the classification of some grass images, as both grass and field images share similarities in their global context. Since four models are trained individually and their convergence shows no signs of overfitting, the absence of cross-validation can be mitigated by the observed stability and consistency. On the MSRSI dataset, the highest misclassification was reported in labeling bridges as overpasses. Additionally, some airport images were misclassified as industrial areas, and rectangular farmland as circular farmland. These results show that the model struggles in instances with high inter-class similarity.

Figure 7 presents the loss graphs (cross-entropy loss) on the UCM, RSSCN7, and MSRSI datasets. The loss graphs indicate overall smooth convergence as the training progresses, showing stable learning behavior across the models. This pattern indicates a reduced likelihood of overfitting during the training process.

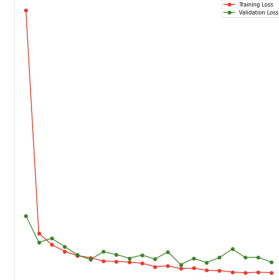
To evaluate the efficacy of the proposed method, we also employed various performance metrics, such as precision, recall, F1-score, false positive rate (FPR), true positive rate (TPR), and Matthews Correlation Coefficient (MCC) [51]. The performance assessment of our proposed method for both datasets is shown in Table 3. The table illustrates that the proposed method achieved an overall adequate performance in each metric, especially for the UCM dataset. It consistently accomplishes a remarkable true positive rate of 100% and a false positive rate of 0%. Additionally, the method demonstrated a high accuracy of 98.10% for the UCM dataset, while still performing well on the RSSCN7 dataset with an accuracy of 94.46%. MCC, regarded as the most reliable metric among the seven compared [52], further supports these results, indicating robust classification performance for both datasets, with values of 98.00% and 93.55% for the UCM and RSSCN7 datasets, respectively. Similarly, the method achieves an accuracy of 95.45% on the MSRSI dataset and an MCC of 95.13%. These results underscore the model’s effectiveness, where it excelled across all evaluated metrics. The high performance on all



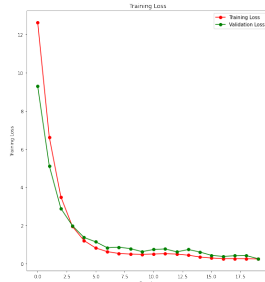
(a) UCM: ViT Base + DenseNet121



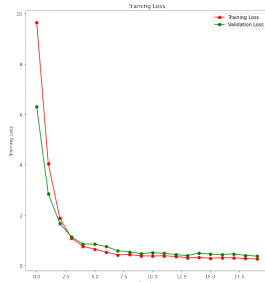
(b) RSSCN7: ViT Base + DenseNet121



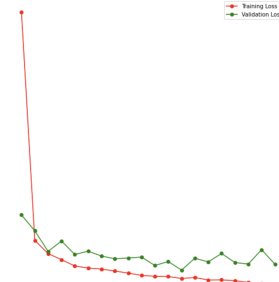
(c) MSRSI: ViT Base + DenseNet121



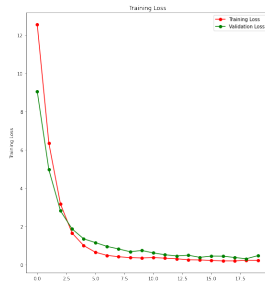
(d) UCM: ViT Base + InceptionResNetV2



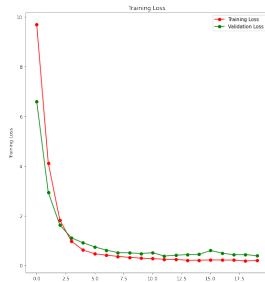
(e) RSSCN7: ViT Base + InceptionResNetV2



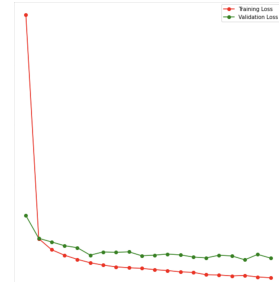
(f) MSRSI: ViT Base + InceptionResNetV2



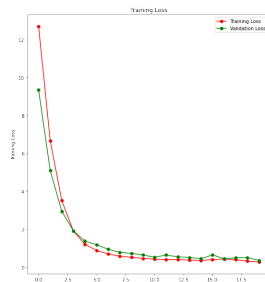
(g) UCM: ViT Base + ResNet152v2



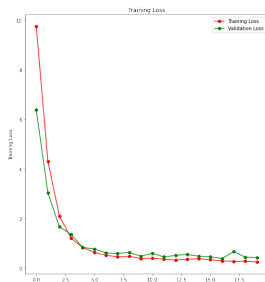
(h) RSSCN7: ViT Base + ResNet152v2



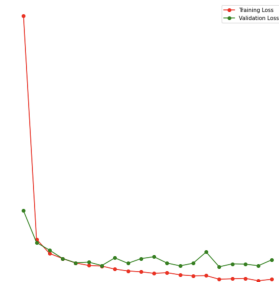
(i) MSRSI: ViT Base + ResNet152v2



(j) UCM: ViT Base + Xception



(k) RSSCN7: ViT Base + Xception



(l) MSRSI: ViT Base + Xception

Figure 7: Loss graphs of four fusion models used for ensembling on the UCM, RSSCN7, and MSRSI datasets.

three datasets suggests the generalizability of the proposed method.

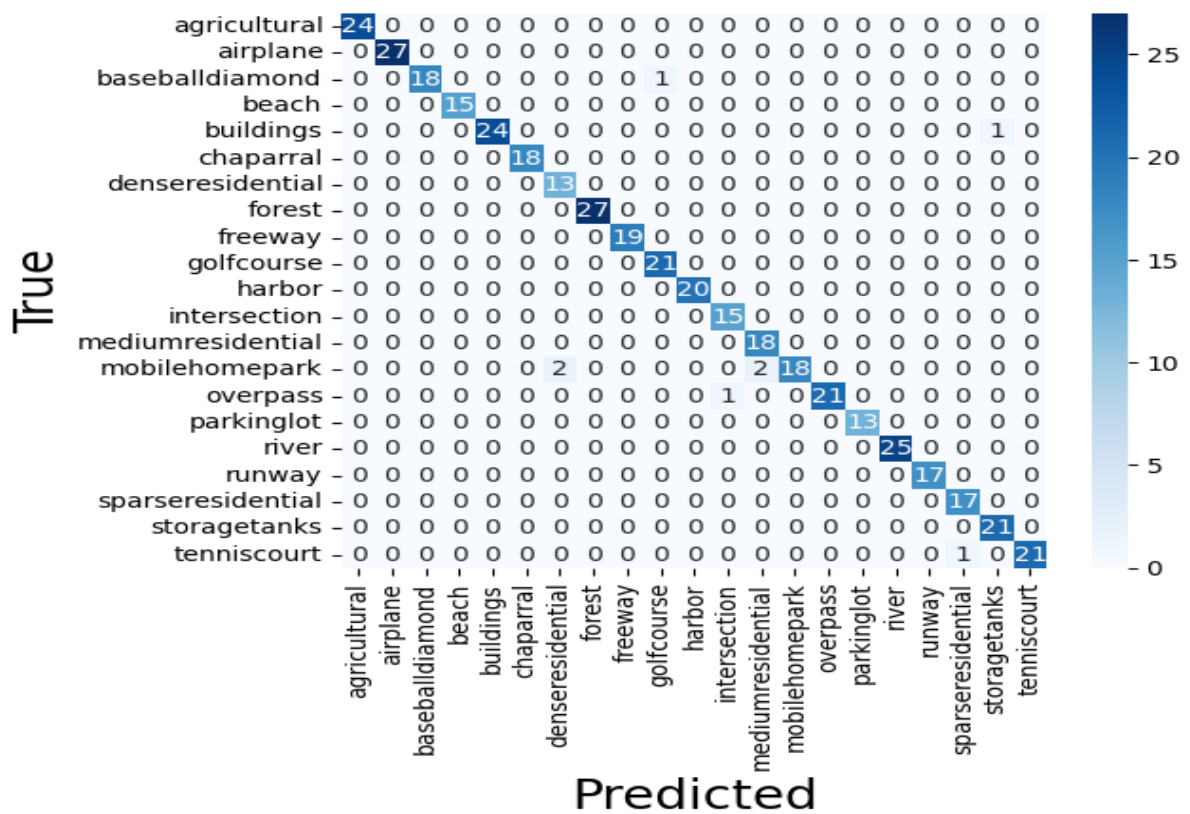


Figure 8: Confusion matrix of the proposed model on the UCM dataset.

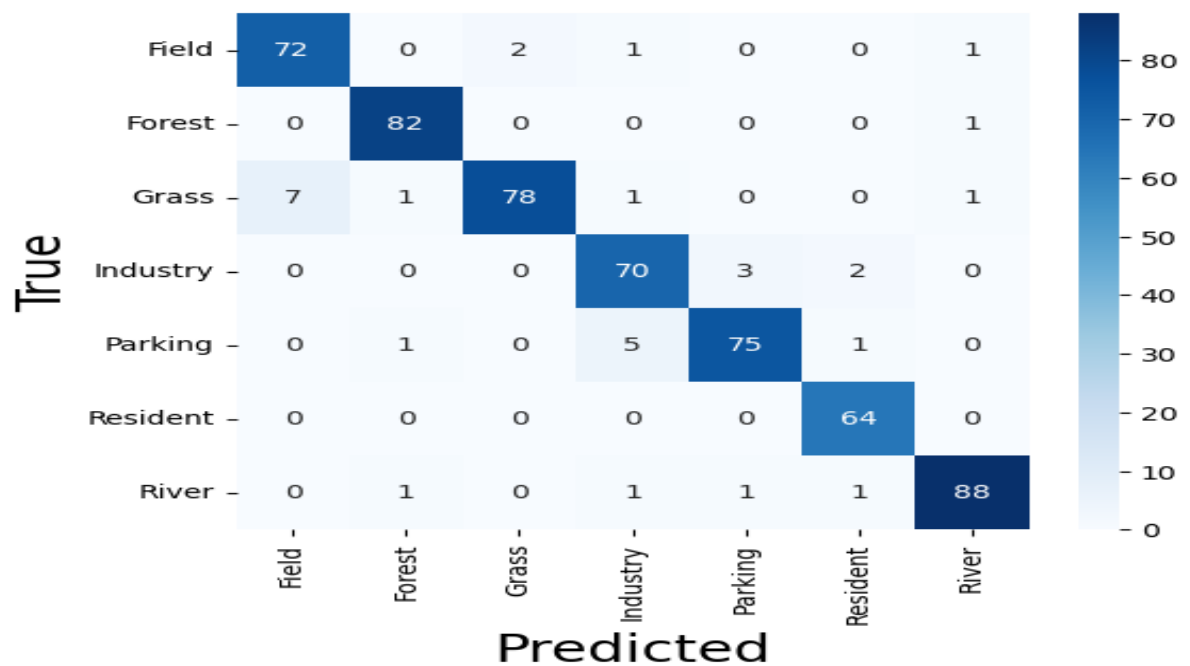


Figure 9: Confusion matrix of the proposed model on the RSSCN7 dataset.

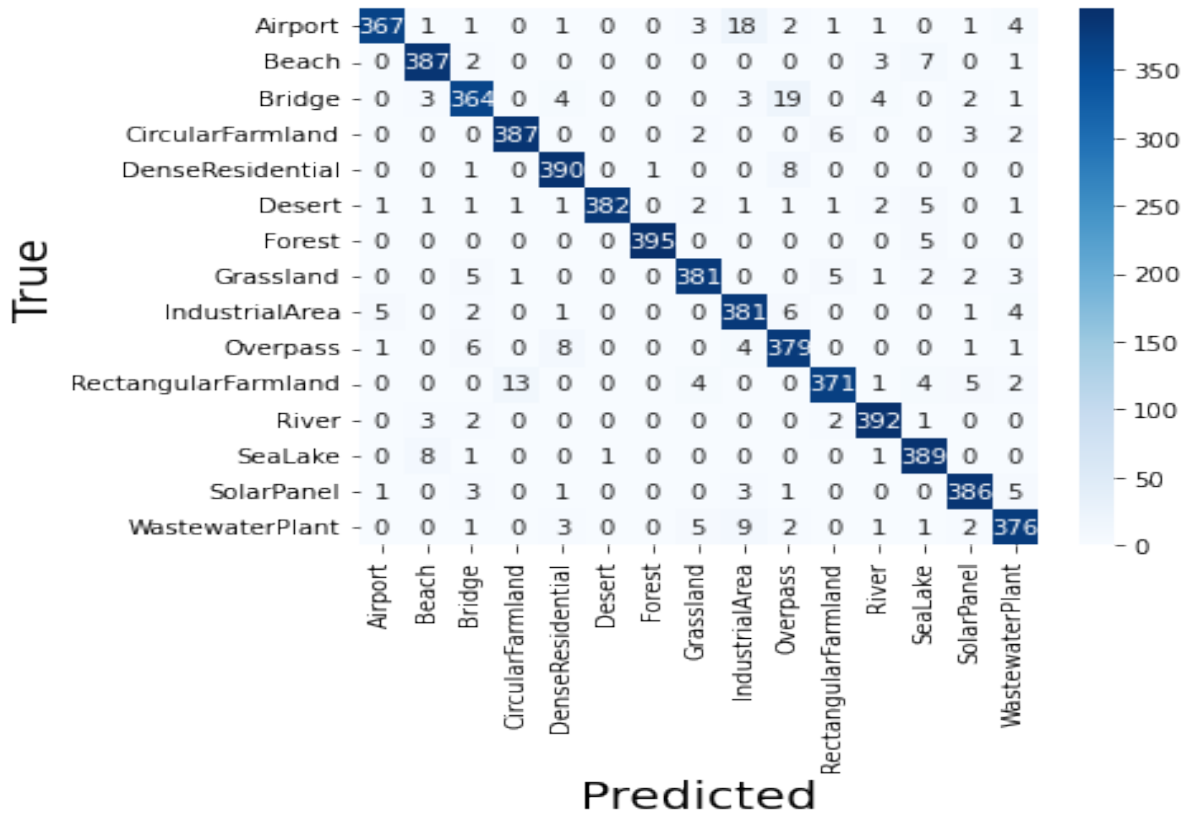


Figure 10: Confusion matrix of the proposed model on the MSRSI dataset.

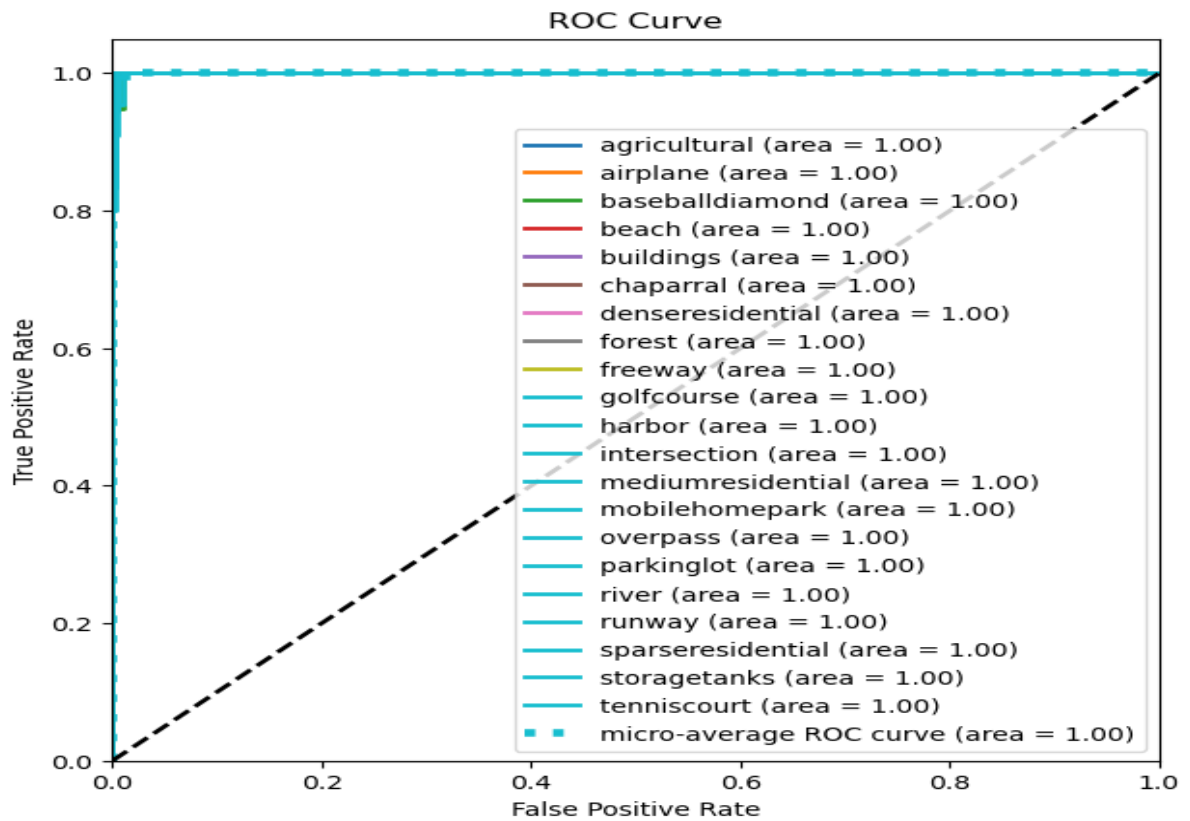


Figure 11: ROC curve of the proposed model on the UCM dataset.

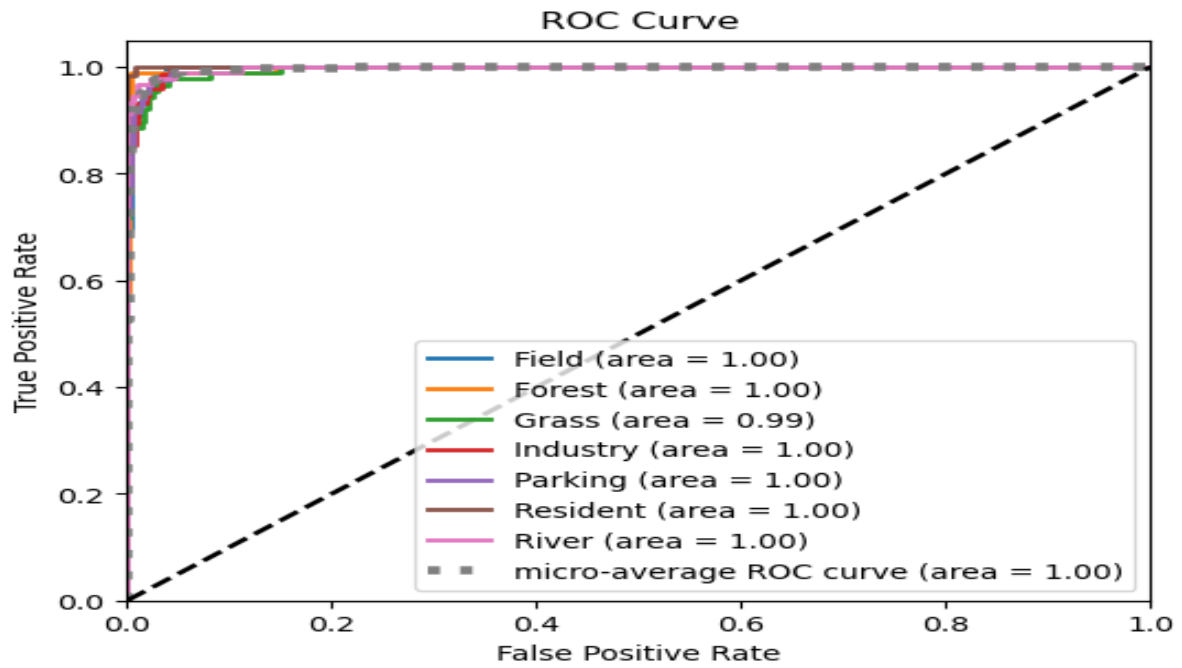


Figure 12: ROC curve of the proposed model on the RSSCN7 dataset.

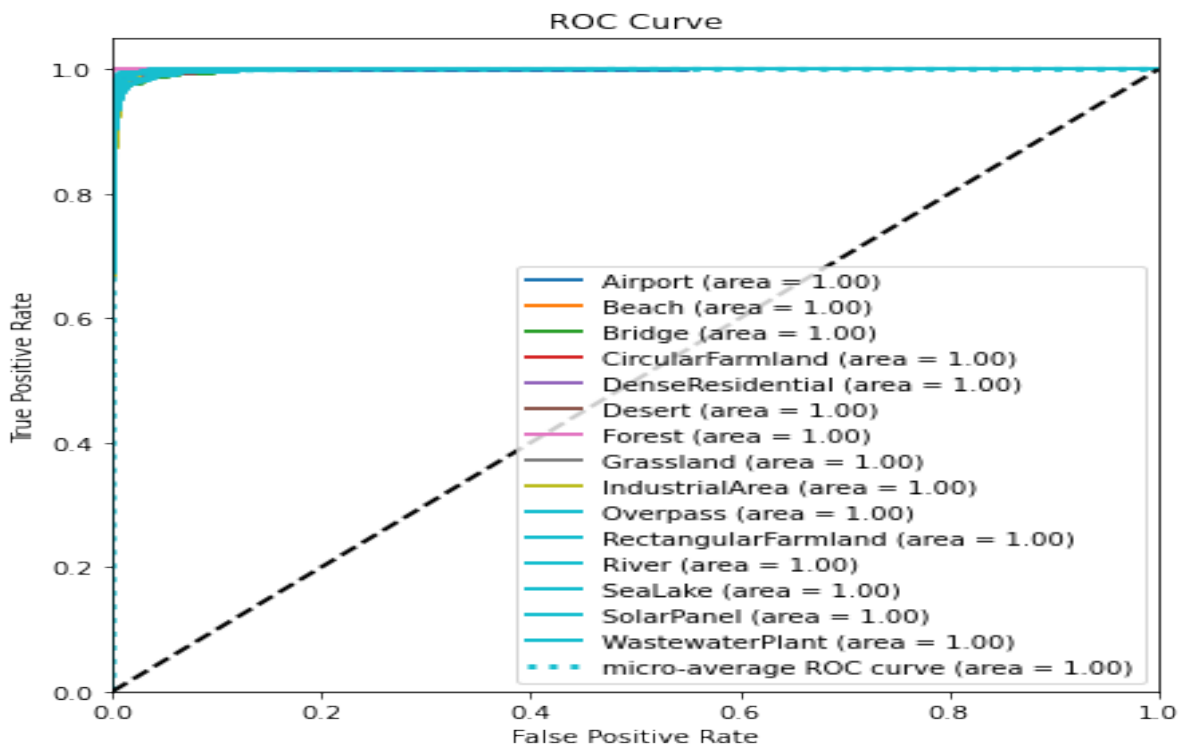


Figure 13: ROC curve of the proposed model on the MSRSI dataset.

Table 3: Performance analysis of the proposed approach.

Measure	UCM	RSSCN7	MSRSI
Accuracy	98.10	94.46	95.45
Precision	98.31	94.61	95.49
Recall	98.10	94.46	95.45
F1-Score	98.11	94.48	95.45
True Positive Rate	100.00	92.13	97.97
False Positive Rate	0.00	4.00	4.18
MCC	98.00	93.55	95.13

Another very effective evaluation parameter is the Receiver Operating Characteristic (ROC) curve. It presents the model’s ability to differentiate between true positive and false positive instances. The ROC curve for the proposed model is present in Figure 11, 12, and 13. The micro average ROC curve on all datasets is 1.0 which is the highest value. This proves the model’s strong discriminate ability. Moreover, in terms of computation, the proposed solution utilizes transfer learning that makes the models train significantly fewer parameters (8.13M) and consumes fewer training epochs (80 epochs in total).

Table 4: Comparison with the state-of-the-art methods.

Model Name	UCM	RSSCN7	MSRSI	Total parameters	Trainable Parameters	Training Epoch
Xception	94.05	87.32	82.13	22.62 M	0.57 M	100
Inception-ResnetV2	92.86	88.57	80.71	54.9 M	0.56 M	100
XCiT	80.95	80.89	71.81	84 M	0.56 M	100
Swin Transformer	95.95	91.79	88.10	195.95 M	0.95 M	100
ViT Base	95.71	89.11	86.55	86.36 M	0.95 M	100
DeiT	90.48	91.07	84.15	86.65 M	0.56 M	100
CLIP - ResNet50	46.43	49.82	34.46	244 M	0	0
CLIP - ViT-L/14	71.42	58.75	68.48	891 M	0	0
SigLIP	72.14	59.64	62.21	400 M	0	0
P ² FEViT	80.48	84.11	59.37	5.63 M	1.58 M	100
Proposed	98.10	94.46	95.45	495.5 M	8.1 M	80

Although making a direct comparison among various research articles is challenging due to the absence of detailed resource consumption information, we have compared our results with state-of-the-art image classifiers. CNNs such as Xception and Inception-ResNetV2, fine-tuned in a similar fashion to the CNN stream of our proposed classifier, have achieved 94.05% and 92.86% accuracy on the UCM dataset, 87.32% and 88.57%

accuracy on the RSSCN7 dataset, and 82.13% and 88.57% on the MSRSI dataset, respectively. Transformer models such as Swin-T and ViT-Base outperformed other variants like XCiT [53] and DeiT by a noticeable margin. Additionally, we have compared our model with Contrastive Language-Image Pretraining (CLIP) [54], a powerful neural network that has outperformed existing CNN and transformer models on various image recognition tasks. The model learns to associate textual descriptions with images by optimizing two encoders (a text and an image encoder). It maximizes the similarity between an image and its corresponding text while minimizing the similarity to unrelated pairs. Once trained, CLIP can generalize to new tasks without additional training, which enables the model to perform zero-shot image classification. We evaluated the model by changing the image encoder, but it failed to produce acceptable accuracy. Notably, although the model does not require any fine-tuning, which is reflected in the trainable parameters, it has one of the highest numbers of parameters due to the integration of two heavy encoder models. Similar to CLIP, we have evaluated another newly developed zero-shot image classifier SigLIP [55]. Similar to CLIP, it fails to achieve notable performance. Lastly, we have evaluated P²FEViT, a hybrid transformer-CNN architecture developed by Wang et al. [56] for remote sensing image classification. Table 4 presents a direct comparison with the models discussed. All the models (except CLIP and SigLIP) were trained for a total of 100 epochs using the same GPU, the P100. Despite the extensive training epochs, these models underperformed compared to our soft voting fusion model, which achieved superior performance after only 20 epochs of training. Although the proposed model has over 495 million parameters, the number of trainable parameters is only 8.1 million. In addition, the model has achieved significantly higher accuracy, particularly on the RSSCN7 and MSRSI datasets.

4.2.1 Ablation Study

On three datasets, UCM, RSSCN7 and MSRSI, Table 5 presents a comparison assessment of the performance of ten different model architectures. The accuracy of the models, which include different Convolutional Neural Networks (CNNs) and Vision Transformers (ViTs), is assessed after a specified number of training epochs. A distinct combination of ViTs and CNNs where the corresponding number of ViTs ranges from 1 to 2 and the number of CNNs ranges from 3 to 6. The models are optimized for fusion-based learning and utilize the improved characteristics of both ViTs and CNNs. On the UCM dataset, the model with 2 ViTs and 5 CNNs obtained the highest accuracy (97.86%), whereas the model with 1 ViT and 5 CNNs had the lowest accuracy (93.86%). On the RSSCN7 dataset, however, accuracy frequently falls lower, with the model with 2 ViTs and 6 CNNs achieving the highest accuracy of 93.75%. On the MSRSI dataset, the top-performing fusion model (1 ViT and 5 CNNs) achieved an accuracy of 88.27%, while

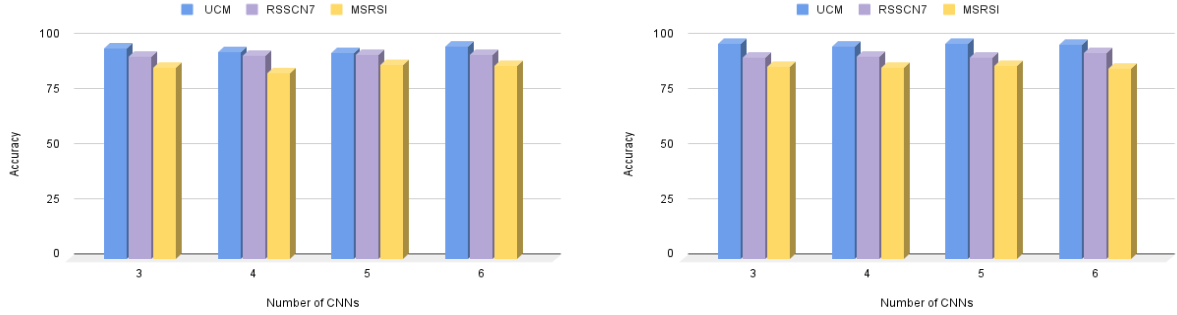
the model with 2 ViTs and 6 CNNs slightly underperformed at 86.73%. The models incorporating one ViT had an average accuracy of 95.19%, 92.56%, and 86.90% on the UCM RSSCN7, and MSRSI datasets, respectively. Notably, employing two ViTs within the models led to average accuracies of 97.63%, 92.19%, and 87.31% on the corresponding datasets. The slight accuracy improvement with two ViTs on UCM and MSRSI but a decrease on RSSCN7 suggests that while multiple ViTs can enhance performance, they may also introduce redundancy or overfitting. In contrast, the models incorporating soft voting had a higher performance than the average of both the one and two ViT models. Additionally, they consumed fewer training resources than other models. All the fusion models performed better than single model classifiers since they can learn from diverse features coming from ViTs and CNNs. Additionally, achieving an accuracy of 98.10% on UCM, 94.46% on RSSCN7 and 95.45 % on MSRSI, the application of soft voting fusion for specific combinations of ViTs and CNNs showed potential.

As shown in Figure 14, it has been noted that the number of ViT and CNN feature extractors has little effect on the overall performance of the fusion model. This phenomenon can be explained by the fact that, after a certain threshold, the extracted features from ViT and CNN tend to overlap as the number of feature extractors rises. The fusion model’s accuracy consequently reaches saturation. Given that ViT and CNN employ various methods to capture meaningful visual data representations, there is a feature overlap between the two systems. While CNN uses convolutional layers to identify local patterns and structures, ViT uses self-attention mechanisms to extract global features from images. The fusion model benefits from a variety of representations obtained from both ViT and CNN in the beginning as the number of feature extractors rises. Beyond a certain point, however, the additional feature extractors begin to extract redundant or extremely similar data to the ones that already exist.

On the other hand, the problem of feature overlapping is resolved when a soft voting scheme is used in the fusion model. Soft voting is a method for combining predictions from different classifiers by giving each prediction a weight and calculating a weighted average. There is no direct overlap of features because soft voting takes each classifier’s individual predictions into account separately. Soft voting’s ability to accommodate a wider range of features that are complementary to one another is a key feature that contributed to the higher performance.

4.3 Comparison with existing works

We have evaluated our proposed solution with some existing literature. A direct comparison of UCM and RSSCN7 datasets is presented in Table 6 and 7, respectively. Notably, since the MSRSI dataset is newly released, no direct comparisons were found. Since both UCM and RSSCN7 datasets are moderately balanced, the researchers relied on accu-



(a) Accuracy over changing the number of CNNs with 1 ViT. (b) Accuracy over changing the number of CNNs with 2 ViTs.

Figure 14: Accuracy over changing number of CNNs and ViTs.

racy as the primary matrix. The majority of the research works have employed transfer learning for the classification of remote sensing images. On the UCM dataset, Thepade et al. [57] presented a deep fusion model that is further fine-tuned with machine learning classifiers. The extensive ablation study presents that InceptionV3 with ExtraTree classifier performs the best. Most of the research works, however, have fine-tuned single feature extractors. Due to the dependence on one feature extractor, some of the models have produced relatively low accuracy.

On the RSSCN7 dataset, however, some researchers have experimented with other approaches. Zhang et al. [62] proposed a compressed network by pruning the unnecessary layers in CNN with an attention mechanism. The compressed network, however, achieved an accuracy of 83.03%. Alhichri et al. [63] fine-tuned several pretrained models for remote sensing image classification. Among them, VGG16 achieved an acceptable 90.87% accuracy. Following the comparison, the proposed model achieved a superior performance over similar approaches.

Since both datasets are moderately balanced, the majority of the research works primarily focused on accuracy as the key evaluation metric. The direct comparison states that the model has the potential to achieve state-of-the-art classification performance. The superiority of the research work lies in the fusion of global and local features which is a crucial part of remote sensing image classification. Additionally, the performance saturation problem was addressed by incorporating the soft voting mechanism. While most research works achieve noteworthy accuracy, they often overlook the efficiency of training resources. Moreover, they mostly neglect thorough error analysis and the integration of Explainable AI techniques, which leaves room for potential biases. This research has carefully addressed both limitations, making a substantial contribution to the remote sensing image classification field.

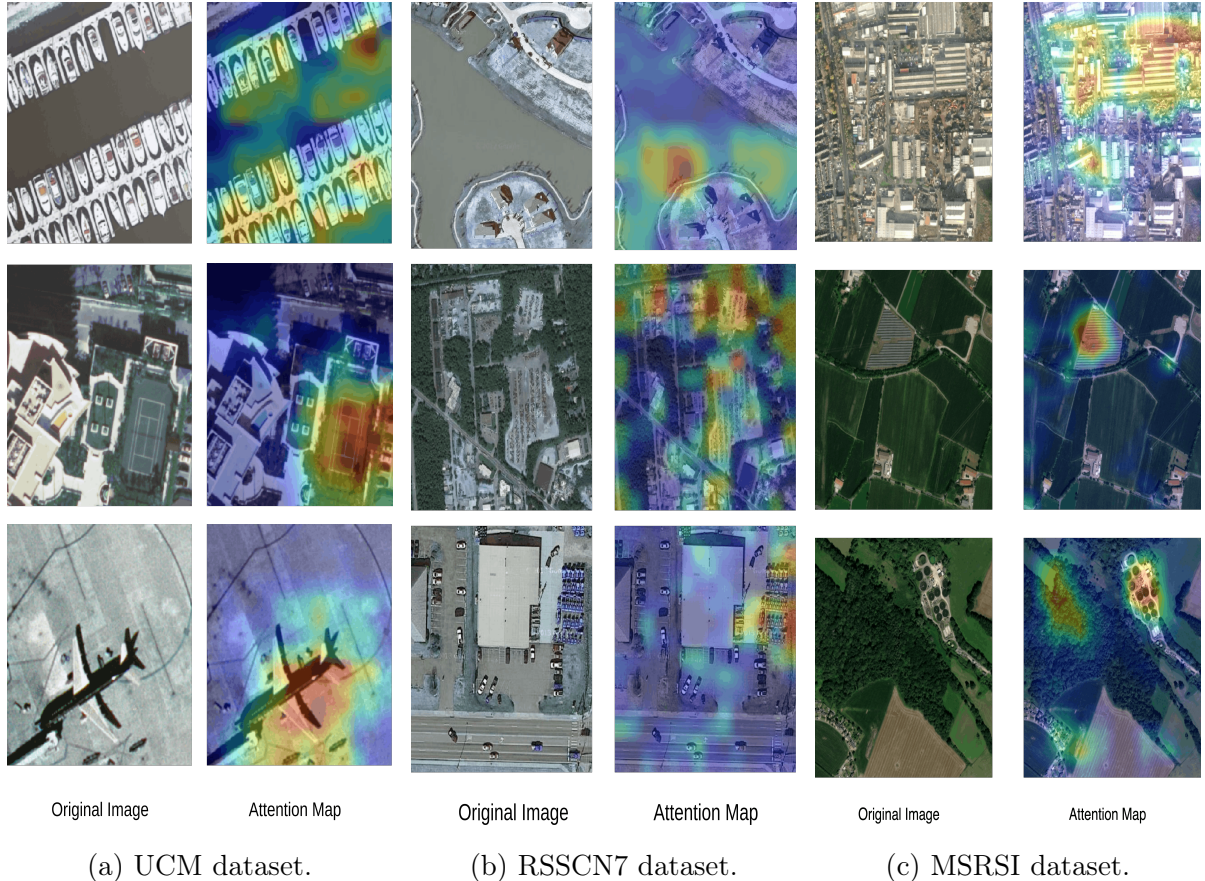


Figure 15: Attention maps of a fusion model on different datasets.

4.4 Explainability and Error Analysis

In view of the comparison presented in Table 6 and 7, the proposed system achieves a competitive accuracy. However, there still remains a need for better model interpretability and bias detection. To understand the model’s decision-making process, we have presented the model’s attention maps. For producing the attention maps, we have leveraged Gradient-weighted Class Activation Mapping (Grad-CAM) [67]. Figure 15a holds the attention heatmap of a fusion model (ViT Base + ResNet152V2) on the UCM dataset. The figure shows that the model has attained the correct regions of the images for making the perfect decision. Likewise, Figure 15b presents the attention heatmap on the RSSCN7 dataset of the same classifier. The examples illustrate that the model prioritizes water features when examining images of rivers. Similarly, the building and the cars are focused on the residents and the parking classes respectively. Likewise, Figure 15c illustrates the attention map on the MSRSI dataset. Similar to the previous examples, the model has correctly focused on the key areas, particularly in the images of the solar panel and wastewater plant.

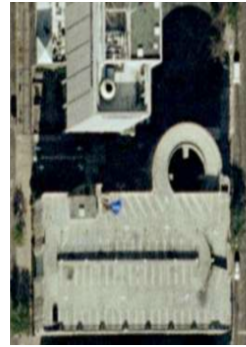
The proposed model, however, makes some incorrect predictions. Figure 16, 17, 18 holds some incorrect predictions of the model on the UCM, RSSCN7, and MSRSI



Actual: Tenniscourt
Predicted: Sparseresidential



Actual: Mobilehomepark
Predicted: Denseresidential



Actual: Buildings
Predicted: Storagetanks



Actual: Baseballdiamond
Predicted: Golfcourse

Figure 16: Error analysis of the proposed model on the UCM dataset.



Actual: Parking
Predicted: Industry



Actual: Industry
Predicted: Resident



Actual: Grass
Predicted: Industry



Actual: Parking
Predicted: Resident

Figure 17: Error analysis of the proposed model on the RSSCN7 dataset.

datasets, respectively. The errors are primarily due to high interclass similarity and little focus on local features. According to the analysis, the model successfully captured global features but struggled with fine-grained details in certain cases. Thus, the global feature became dominant and adversely influenced the classification.

4.5 Discussion

We have developed an ensemble model combining two-stream fusion models, where each model has classification ability. The architecture of the model is carefully designed to be resource-efficient while training. A comparative study demonstrates the superior performance of the proposed solution. Notably, the proposed solution leverages existing techniques like CNN and ViT. Nonetheless, the major contribution of this research lies in the effective integration of these modules. Our study shows that combining ViT and CNNs leads to performance saturation due to overlapping feature extraction, which can be mitigated through soft voting. Additionally, we have shown that instead of training large models with a high number of epochs, training smaller models with fewer epochs



Figure 18: Error analysis of the proposed model on the MSRSI dataset.

and combining their predictions through a voting mechanism is an effective solution that elevates the performance and reduces resource consumption. However, due to the integration of four fusion models, the model consumes relatively high memory while testing. Nevertheless, since the four models have independent classification abilities, the inference process can be parallelized by running each fusion model separately. Furthermore, the models can be compressed using different techniques, including quantization and pruning. Since compression techniques can potentially degrade performance, a comprehensive study is needed to ensure that performance is maintained while minimizing resource consumption. Lastly, although the architecture is primarily designed for classifying remote sensing images, its strong discriminative capability makes it suitable for other applications as well—such as remote sensing image retrieval, with minimal modifications. To enable retrieval, the class label can be encoded and fused with the extracted image features, resulting in a compact and informative representation of the remote sensing data as demonstrated in previous works [68–70]. Overall, the model can be a reliable option for remote sensing image classification, considering the performance and the computational efficiency of training.

Table 5: Comparison with different methods.

Model Type	Model Structure	No of ViTs	No of CNNs	UCM	RSS-CN7	MS-RSI	Epo-chs
Fusion	ViT Base + Xception + ResNet152v2 + MobileNetV3Large	1	3	95.95	92.14	86.83	100
Fusion	ViT Base + Xception + ResNet152v2 + MobileNetV3Large + EfficientNetB7	1	4	94.29	92.57	84.70	100
Fusion	ViT Base + Xception + ResNet152v2 + MobileNetV3Large + EfficientNetB7 + DenseNet121	1	5	93.86	92.68	88.27	100
Fusion	ViT Base + InceptionResNetV2 + DenseNet121 + EfficientNetB7 + Xception + ResNet152v2 + MobileNetV3Large	1	6	96.67	92.86	87.78	100
Fusion	ViT Base + ViT Large + Xception + ResNet152v2 + MobileNetV3Large	2	3	97.86	91.43	87.55	100
Fusion	ViT Base + ViT Large + Xception + ResNet152v2 + MobileNetV3Large + EfficientNetB7	2	4	96.43	92.14	87.20	100
Fusion	ViT Base + ViT Large + DenseNet121 + Xception + ResNet152v2 + MobileNetV3Large + EfficientNetB7	2	5	97.86	91.43	87.77	100
Fusion	ViT Base + ViT Large + InceptionResNetV2 + DenseNet121 + EfficientNetB7 + Xception + ResNet152v2 + MobileNetV3Large	2	6	97.38	93.75	86.73	100
Fusion + Soft Voting	(ViT Base + DenseNet121), (ViT Base + ResNet152v2)	2	2	98.10	92.86	94.87	40
Fusion + Soft Voting	(ViT Base+DenseNet121), (ViT Base+ResNet152v2), (ViT Base+InceptionResNetV2), (ViT Base+Xception)	4	4	98.10	94.46	95.45	80

Table 6: Comparison of different models on UCM dataset.

Model	Accuracy	Precision	Recall	F1-Score
Snapshot ensemble CNN, dropCycle [58]	97.38	-	-	-
Residual Network-based Features Extraction, Self-adaptive Global Best Harmony Search [59]	97.92	-	-	-
InceptionV3, Thepade’s Sorted Block Truncation Coding, ExtraTree [57]	98.33	98.42	98.33	98.32
Custom Shallow CNN [18]	88.1	89.9	88	89
ResNet50 with Channel Attention [60]	98.68	-	-	-
Multi-level Convolutional Pyramid Semantic Fusion [61]	97.54	-	-	-
Proposed	98.10	98.31	98.10	98.11

Table 7: Comparison of different models on RSSCN7 dataset.

Model	Accuracy	Precision	Recall	F1-Score
Node Entropy [35]	89.39	-	-	-
Representation Learning, Resnet 50 [64]	91.52	-	-	-
Deep Color Fusion [65]	92.9	-	-	-
Filter Pruning With attention mechanism [62]	83.93	-	-	-
VGG16 [63]	90.87	-	-	-
Visual representation cross entropy [66]	94	95	93	93
Proposed	94.46	94.61	94.46	94.48

5 Conclusion

In this research, a novel and efficient architecture is presented for classifying the remote sensing images. The introducing model combines CNN architecture with Vision Transformers (ViTs), and in order to increase the prediction probability, soft voting is also used. The proposed fusion model successfully capitalizes on the expertise of both CNNs and ViTs, as well as the benefits of the soft voting mechanism to produce a robust classifier. The UC Merced Land Use (UCM), RSSCN7, and MSRSI datasets were used to thoroughly evaluate the model. The dataset is balanced using geometric augmentation, and the gamma transformation is applied to enhance the image quality. The results obtained for these datasets, 98.10%, 94.46%, and 95.45%, respectively, demonstrate outstanding efficacy in identifying different types of remote sensing images. The accuracy attained by the model demonstrates its ability to handle diversified land cover classes and remote sensing images. A comparison assessment with different models is performed and it is observed that the proposed fusion model outperforms other architectures substantially, showing its superiority in classification tasks. The evaluation metrics also further validate the model's stability and reliability. This system, however, consumes a relatively high amount of memory, which can be compressed using quantization techniques. Nonetheless, these techniques may lead to a reduction in classification accuracy. In the future, a study could be conducted to reduce memory consumption without compromising performance. In conclusion, the suggested fusion model represents a substantial development in classifying remote sensing images. It establishes new opportunities for utilizing deep learning's potential in various remote sensing applications. The fusion of these two architectures offers a comprehensive solution to address the challenges of classifying a large-scale image and contributes to the exploration and knowledge extraction from remote sensing data.

Supplementary Materials

The experiment can be found at this link: <https://github.com/NifulIslam/Remote-Sensing-Image-Classification-With-ViT-and-CNN/tree/main>. The readme file presents the detailed methodology at a glance.

References

- [1] Wadii Boulila, Mokhtar Sellami, Maha Driss, Mohammed Al-Sarem, Mahmood Safaei, and Fuad A Ghaleb. Rs-dcnn: A novel distributed convolutional-neural-networks based-approach for big remote-sensing image classification. *Computers and Electronics in Agriculture*, 182:106014, 2021.

- [2] Yakoub Bazi, Laila Bashmal, Mohamad M Al Rahhal, Reham Al Dayil, and Naif Al Ajlan. Vision transformers for remote sensing image classification. *Remote Sensing*, 13(3):516, 2021.
- [3] Maryam Mehmood, Ahsan Shahzad, Bushra Zafar, Amsa Shabbir, and Nouman Ali. Remote sensing image classification: A comprehensive review and applications. *Mathematical Problems in Engineering*, 2022:1–24, 2022.
- [4] Andrea Maracani, Vito Paolo Pastore, Lorenzo Natale, Lorenzo Rosasco, and Francesca Odone. In-domain versus out-of-domain transfer learning in plankton image classification. *Scientific Reports*, 13(1):10443, 2023.
- [5] Saksham Gupta, Satvik Agrawal, Sunil K Singh, and Sudhakar Kumar. A novel transfer learning-based model for ultrasound breast cancer image classification. In *Computational Vision and Bio-Inspired Computing: Proceedings of ICCVBIC 2022*, pages 511–523. Springer, 2023.
- [6] Mohammad Najjartabar Bisheh, Xinya Wang, Shing I Chang, Shuting Lei, and Jianfeng Ma. Image-based characterization of laser scribing quality using transfer learning. *Journal of Intelligent Manufacturing*, 34(5):2307–2319, 2023.
- [7] Yogesh Kumar and Surbhi Gupta. Deep transfer learning approaches to predict glaucoma, cataract, choroidal neovascularization, diabetic macular edema, drusen and healthy eyes: an experimental review. *Archives of Computational Methods in Engineering*, 30(1):521–541, 2023.
- [8] Qiqi He, Qiuju Yang, and Minghao Xie. Hctnet: A hybrid cnn-transformer network for breast ultrasound image segmentation. *Computers in Biology and Medicine*, 155:106629, 2023.
- [9] Alexey Dosovitskiy, Lucas Beyer, Alexander Kolesnikov, Dirk Weissenborn, Xiaohua Zhai, Thomas Unterthiner, Mostafa Dehghani, Matthias Minderer, Georg Heigold, Sylvain Gelly, et al. An image is worth 16x16 words: Transformers for image recognition at scale. *arXiv preprint arXiv:2010.11929*, 2020.
- [10] Ashish Vaswani, Noam Shazeer, Niki Parmar, Jakob Uszkoreit, Llion Jones, Aidan N Gomez, Łukasz Kaiser, and Illia Polosukhin. Attention is all you need. *Advances in neural information processing systems*, 30, 2017.
- [11] Hugo Touvron, Matthieu Cord, Matthijs Douze, Francisco Massa, Alexandre Sablayrolles, and Hervé Jégou. Training data-efficient image transformers & distillation through attention. In *International conference on machine learning*, pages 10347–10357. PMLR, 2021.

- [12] Ze Liu, Yutong Lin, Yue Cao, Han Hu, Yixuan Wei, Zheng Zhang, Stephen Lin, and Baining Guo. Swin transformer: Hierarchical vision transformer using shifted windows. In *Proceedings of the IEEE/CVF international conference on computer vision*, pages 10012–10022, 2021.
- [13] Xiao Jiang, Yaxin Zhang, Mian Pan, Shuaishuai Lv, Gang Yang, Zhu Li, Jingbiao Liu, and Haibin Yu. A marine organism detection framework based on dataset augmentation and cnn-vit fusion. *Journal of Marine Science and Engineering*, 11(4):705, 2023.
- [14] Junge Shen, Tianwei Yu, Haopeng Yang, Ruxin Wang, and Qi Wang. An attention cascade global–local network for remote sensing scene classification. *Remote Sensing*, 14(9):2042, 2022.
- [15] Anwer Mustafa Hilal, Fahd N Al-Wesabi, Khalid J Alzahrani, Mesfer Al Duhayyim, Manar Ahmed Hamza, Mohammed Rizwanullah, and Vicente García Díaz. Deep transfer learning based fusion model for environmental remote sensing image classification model. *European Journal of Remote Sensing*, 55(sup1):12–23, 2022.
- [16] Wei Huang, Yilei Shi, Zhitong Xiong, Qi Wang, and Xiao Xiang Zhu. Semi-supervised bidirectional alignment for remote sensing cross-domain scene classification. *ISPRS Journal of Photogrammetry and Remote Sensing*, 195:192–203, 2023.
- [17] Yazeed Yasin Ghadi, Adnan Ahmed Rafique, Tamara Al Shloul, Suliman A Al-suhibany, Ahmad Jalal, and Jeongmin Park. Robust object categorization and scene classification over remote sensing images via features fusion and fully convolutional network. *Remote Sensing*, 14(7):1550, 2022.
- [18] Abebaw Alem and Shailender Kumar. Deep learning models performance evaluations for remote sensed image classification. *IEEE Access*, 10:111784–111793, 2022.
- [19] Mohammed Al-Jabbar, Ebtessam Al-Mansor, S Abdel-Khalek, and Salem Alkhalaf. Ebola optimization with modified darknet-53 model for scene classification and security on internet of things in smart cities. *Alexandria Engineering Journal*, 75:29–40, 2023.
- [20] S Thirumaladevi, K Veera Swamy, and M Sailaja. Remote sensing image scene classification by transfer learning to augment the accuracy. *Measurement: Sensors*, 25:100645, 2023.
- [21] VN Vinaykumar, J Ananda Babu, and Jaroslav Frnda. Optimal guidance whale optimization algorithm and hybrid deep learning networks for land use land cover classification. *EURASIP Journal on Advances in Signal Processing*, 2023(1):13, 2023.

- [22] Xinyu Wang, Haixia Xu, Liming Yuan, Wei Dai, and Xianbin Wen. A remote-sensing scene-image classification method based on deep multiple-instance learning with a residual dense attention convnet. *Remote Sensing*, 14(20):5095, 2022.
- [23] Guowei Wang, Haixia Xu, Xinyu Wang, Liming Yuan, and Xianbin Wen. Remote sensing scene image classification model based on multi-scale features and attention mechanism. *Journal of Applied Remote Sensing*, 16(4):044510–044510, 2022.
- [24] Junjie Wang, Wei Li, Mengmeng Zhang, and Jocelyn Chanussot. Large kernel sparse convnet weighted by multi-frequency attention for remote sensing scene understanding. *IEEE Transactions on Geoscience and Remote Sensing*, 61:1–12, 2023.
- [25] Junjie Wang, Wei Li, Mengmeng Zhang, Ran Tao, and Jocelyn Chanussot. Remote sensing scene classification via multi-stage self-guided separation network. *IEEE Transactions on Geoscience and Remote Sensing*, 2023.
- [26] Mengmeng Zhang, Wei Li, Xudong Zhao, Huan Liu, Ran Tao, and Qian Du. Morphological transformation and spatial-logical aggregation for tree species classification using hyperspectral imagery. *IEEE Transactions on Geoscience and Remote Sensing*, 61:1–12, 2023.
- [27] Souleyman Chaib, Dou El Kefel Mansouri, Ibrahim Omara, Ahmed Hagag, Sahraoui Dhelim, and Djamel Amar Bensaber. On the co-selection of vision transformer features and images for very high-resolution image scene classification. *Remote Sensing*, 14(22):5817, 2022.
- [28] Siyuan Hao, Bin Wu, Kun Zhao, Yuanxin Ye, and Wei Wang. Two-stream swin transformer with differentiable sobel operator for remote sensing image classification. *Remote Sensing*, 14(6):1507, 2022.
- [29] Kejie Xu, Peifang Deng, and Hong Huang. Vision transformer: An excellent teacher for guiding small networks in remote sensing image scene classification. *IEEE Transactions on Geoscience and Remote Sensing*, 60:1–15, 2022.
- [30] Swalpa Kumar Roy, Ankur Deria, Danfeng Hong, Behnood Rasti, Antonio Plaza, and Jocelyn Chanussot. Multimodal fusion transformer for remote sensing image classification. *IEEE Transactions on Geoscience and Remote Sensing*, 61:1–20, 2023.
- [31] Fulin Xu, Shaohui Mei, Ge Zhang, Nan Wang, and Qian Du. Bridging cnn and transformer with cross attention fusion network for hyperspectral image classification. *IEEE Transactions on Geoscience and Remote Sensing*, 2024.

- [32] Huiqing Wang, Huajun Wang, and Linfen Wu. Tgf-net: Transformer and gist cnn fusion network for multi-modal remote sensing image classification. *PloS one*, 20(2):e0316900, 2025.
- [33] Sichao Fu, Weifeng Liu, Kai Zhang, and Yicong Zhou. Example-feature graph convolutional networks for semi-supervised classification. *Neurocomputing*, 461:63–76, 2021.
- [34] Yunlong Yu, Xianzhi Li, and Fuxian Liu. Attention gans: Unsupervised deep feature learning for aerial scene classification. *IEEE Transactions on Geoscience and Remote Sensing*, 58(1):519–531, 2019.
- [35] Jiachen Yang, Yue Yang, Jiabao Wen, Yang Li, and Sezai Ercisli. Remote sensing image information quality evaluation via node entropy for efficient classification. *Remote Sensing*, 14(17):4400, 2022.
- [36] Sreenath P Kyathanahally, Thomas Hardeman, Marta Reyes, Ewa Merz, Thea Bulas, Philipp Brun, Francesco Pomati, and Marco Baity-Jesi. Ensembles of data-efficient vision transformers as a new paradigm for automated classification in ecology. *Scientific Reports*, 12(1):18590, 2022.
- [37] Zhenghao Wei. Ensemble model of visual transformer and cnn helps ba diagnosis for doctors in underdeveloped areas. In *Proceedings of the Asian Conference on Computer Vision*, pages 68–84, 2022.
- [38] SM Nabil Ashraf, Md Adyelullahil Mamun, Hasnat Md Abdullah, and Md Golam Rabiul Alam. Synthensemble: A fusion of cnn, vision transformer, and hybrid models for multi-label chest x-ray classification. In *2023 26th International Conference on Computer and Information Technology (ICCIT)*, pages 1–6. IEEE, 2023.
- [39] Haiping Wu, Bin Xiao, Noel Codella, Mengchen Liu, Xiyang Dai, Lu Yuan, and Lei Zhang. Cvt: Introducing convolutions to vision transformers. In *Proceedings of the IEEE/CVF international conference on computer vision*, pages 22–31, 2021.
- [40] Ajay Sharma and Pramod Kumar Mishra. Image enhancement techniques on deep learning approaches for automated diagnosis of covid-19 features using cxr images. *Multimedia Tools and Applications*, 81(29):42649–42690, 2022.
- [41] Ahmed Magdy, Hadeer Hussein, Rehab F Abdel-Kader, and Khaled Abd El Salam. Performance enhancement of skin cancer classification using computer vision. *IEEE Access*, 2023.

- [42] Jie Hu, Li Shen, and Gang Sun. Squeeze-and-excitation networks. In *Proceedings of the IEEE conference on computer vision and pattern recognition*, pages 7132–7141, 2018.
- [43] Gao Huang, Zhuang Liu, Laurens Van Der Maaten, and Kilian Q Weinberger. Densely connected convolutional networks. In *Proceedings of the IEEE conference on computer vision and pattern recognition*, pages 4700–4708, 2017.
- [44] Kaiming He, Xiangyu Zhang, Shaoqing Ren, and Jian Sun. Deep residual learning for image recognition. In *Proceedings of the IEEE conference on computer vision and pattern recognition*, pages 770–778, 2016.
- [45] Christian Szegedy, Sergey Ioffe, Vincent Vanhoucke, and Alexander Alemi. Inception-v4, inception-resnet and the impact of residual connections on learning. In *Proceedings of the AAAI conference on artificial intelligence*, volume 31, 2017.
- [46] François Chollet. Xception: Deep learning with depthwise separable convolutions. In *Proceedings of the IEEE conference on computer vision and pattern recognition*, pages 1251–1258, 2017.
- [47] Byung Chul Kim, Hoe Chang Kim, Sungho Han, and Dong Kyou Park. Inspection of underwater hull surface condition using the soft voting ensemble of the transfer-learned models. *Sensors*, 22(12):4392, 2022.
- [48] Yi Yang and Shawn Newsam. Bag-of-visual-words and spatial extensions for land-use classification. In *Proceedings of the 18th SIGSPATIAL international conference on advances in geographic information systems*, pages 270–279, 2010.
- [49] Nouman Ali, Bushra Zafar, Faisal Riaz, Saadat Hanif Dar, Naeem Iqbal Ratyal, Khalid Bashir Bajwa, Muhammad Kashif Iqbal, and Muhammad Sajid. A hybrid geometric spatial image representation for scene classification. *PloS one*, 13(9):e0203339, 2018.
- [50] Yuxi Sun, Yunming Ye, Jian Kang, Ruben Fernandez-Beltran, Xutao Li, Zhenyu Xiong, Xu Huang, and Antonio Plaza. Consistency center-based deep cross-modal hashing for multisource remote sensing image retrieval. *IEEE Transactions on Geoscience and Remote Sensing*, 61:1–16, 2023.
- [51] Ž Vujović et al. Classification model evaluation metrics. *International Journal of Advanced Computer Science and Applications*, 12(6):599–606, 2021.
- [52] Davide Chicco, Niklas Töttsch, and Giuseppe Jurman. The matthews correlation coefficient (mcc) is more reliable than balanced accuracy, bookmaker informedness,

- and markedness in two-class confusion matrix evaluation. *BioData mining*, 14:1–22, 2021.
- [53] Alaaeldin Ali, Hugo Touvron, Mathilde Caron, Piotr Bojanowski, Matthijs Douze, Armand Joulin, Ivan Laptev, Natalia Neverova, Gabriel Synnaeve, Jakob Verbeek, et al. Xcit: Cross-covariance image transformers. *Advances in neural information processing systems*, 34:20014–20027, 2021.
- [54] Alec Radford, Jong Wook Kim, Chris Hallacy, Aditya Ramesh, Gabriel Goh, Sandhini Agarwal, Girish Sastry, Amanda Askell, Pamela Mishkin, Jack Clark, et al. Learning transferable visual models from natural language supervision. In *International conference on machine learning*, pages 8748–8763. PMLR, 2021.
- [55] Xiaohua Zhai, Basil Mustafa, Alexander Kolesnikov, and Lucas Beyer. Sigmoid loss for language image pre-training. In *Proceedings of the IEEE/CVF international conference on computer vision*, pages 11975–11986, 2023.
- [56] Guanqun Wang, He Chen, Liang Chen, Yin Zhuang, Shanghang Zhang, Tong Zhang, Hao Dong, and Peng Gao. P2fevit: Plug-and-play cnn feature embedded hybrid vision transformer for remote sensing image classification. *Remote Sensing*, 15(7):1773, 2023.
- [57] Sudeep D Thepade and Mayuresh R Dindorkar. Fusing deep convolutional neural network features with thepade’s sbtc for land usage identification. *Engineering Science and Technology, an International Journal*, 27:101014, 2022.
- [58] Sangdaow Noppitak and Olarik Surinta. dropcyclic: snapshot ensemble convolutional neural network based on a new learning rate schedule for land use classification. *IEEE Access*, 10:60725–60737, 2022.
- [59] Aghila Rajagopal, A Ramachandran, K Shankar, Manju Khari, Sudan Jha, Yongju Lee, and Gyanendra Prasad Joshi. Fine-tuned residual network-based features with latent variable support vector machine-based optimal scene classification model for unmanned aerial vehicles. *IEEE Access*, 8:118396–118404, 2020.
- [60] Zheng Zhuo and Zhong Zhou. Remote sensing image retrieval with gabor-ca-resnet and split-based deep feature transform network. *Remote Sensing*, 13(5):869, 2021.
- [61] Xiongli Sun, Qiqi Zhu, and Qianqing Qin. A multi-level convolution pyramid semantic fusion framework for high-resolution remote sensing image scene classification and annotation. *IEEE Access*, 9:18195–18208, 2021.

- [62] Shuo Zhang, Gengshen Wu, Junhua Gu, and Jungong Han. Pruning convolutional neural networks with an attention mechanism for remote sensing image classification. *Electronics*, 9(8):1209, 2020.
- [63] Haikel Alhichri. Rs-deepsuperlearner: fusion of cnn ensemble for remote sensing scene classification. *Annals of GIS*, 29(1):121–142, 2023.
- [64] Wenyuan Li, Keyan Chen, Hao Chen, and Zhenwei Shi. Geographical knowledge-driven representation learning for remote sensing images. *IEEE Transactions on Geoscience and Remote Sensing*, 60:1–16, 2021.
- [65] Rao Muhammad Anwer, Fahad Shahbaz Khan, and Jorma Laaksonen. Compact deep color features for remote sensing scene classification. *Neural Processing Letters*, 53(2):1523–1544, 2021.
- [66] Denghui Zhang, Muhammad Shafiq, Ligu Wang, Gautam Srivastava, and Shoulin Yin. Privacy-preserving remote sensing images recognition based on limited visual cryptography. *CAAI Transactions on Intelligence Technology*, 2023.
- [67] Ramprasaath R Selvaraju, Michael Cogswell, Abhishek Das, Ramakrishna Vedantam, Devi Parikh, and Dhruv Batra. Grad-cam: Visual explanations from deep networks via gradient-based localization. In *Proceedings of the IEEE international conference on computer vision*, pages 618–626, 2017.
- [68] Jian Kang, Ruben Fernandez-Beltran, Zhen Ye, Xiaohua Tong, and Antonio Plaza. Deep hashing based on class-discriminated neighborhood embedding. *IEEE Journal of Selected Topics in Applied Earth Observations and Remote Sensing*, 13:5998–6007, 2020.
- [69] Yuxi Sun, Shanshan Feng, Yunming Ye, Xutao Li, Jian Kang, Zhichao Huang, and Chuyao Luo. Multisensor fusion and explicit semantic preserving-based deep hashing for cross-modal remote sensing image retrieval. *IEEE Transactions on Geoscience and Remote Sensing*, 60:1–14, 2021.
- [70] Yuxi Sun, Yunming Ye, Xutao Li, Shanshan Feng, Bowen Zhang, Jian Kang, and Kuai Dai. Unsupervised deep hashing through learning soft pseudo label for remote sensing image retrieval. *Knowledge-Based Systems*, 239:107807, 2022.